Selective Oxidation of 1,2-Propanediol in Alkaline Anion-Exchange Membrane Electrocatalytic Flow Reactors: Experimental and DFT Investigations

David J. Chadderdon,[†,∥,⊥] Le Xin,[†,⊥] Ji Qi,[†,∥] Brian Brady,[‡] Julie A. Miller,[‡] Kai Sun,[§] Michael J. Janik,*[,‡] and Wenzhen Li*[,†,∥]

[†]Department of Chemical Engineering Michigan Technological University, Houghton, Michigan 49931, United States
[‡]Department of Chemical Engineering Pennsylvania State University, University Park, Pennsylvania 16802, United States
[§]Department of Material Science and Engineering University of Michigan, Ann Arbor, Michigan 48109, United States

Ⓢ *Supporting Information*

ABSTRACT: Electrocatalytic oxidation of polyhydric alcohols represents an important route for coproduction of biorenewable chemicals and energy. However, the governing factors leading to high product selectivity remain unclear. Herein, we investigate the selective oxidation of 1,2-propanediol (PDO) to pyruvate or lactate in electrocatalytic reactors over carbon-supported platinum (Pt/C) and gold (Au/C) anode catalysts. PDO-fed alkaline anion-exchange membrane fuel cells successfully cogenerated electricity and valuable chemicals with peak power densities of 46.3 mW cm^{-2} on Pt/C and 10.0 mW cm^{-2} on Au/C. Pt/C was highly selective for primary alcohol group oxidation to lactate (86.8%) under fuel cell conditions, but Au/C yielded significant amounts of pyruvate, a product that has previously eluded heterogeneous catalytic studies on Au. Sequential oxidation of lactate to pyruvate was not observed on Au/C but did occur slowly on Pt/C. The electrode potential dependent product distribution was investigated, and it was revealed that pyruvate selectivity on Au/C was sensitive to anode potential and could be varied from 20 to 56%. On the basis of observed product distributions and linear sweep voltammetry of intermediate products, we propose that the intermediates hydroxyacetone and pyruvaldehyde, which are not stable in high pH electrolyte, can be further oxidized to pyruvate on Au/C only if they are trapped within the thick liquid diffusion layer of the carbon cloth supported catalyst layer. Density functional theory (DFT) calculations of reaction energies identified the most favorable reaction intermediates and provided insight into the likely reaction pathways.

KEYWORDS: selective oxidation, 1,2-propanediol, pyruvic acid, lactic acid, fuel cells, DFT
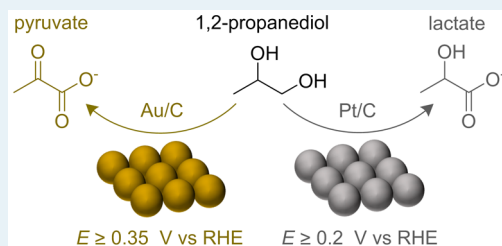
1. INTRODUCTION

Renewable biomass has received great interest for its potential to replace petroleum as the primary feedstock for liquid fuels, chemicals, and polymeric materials. Biodiesel made by the transesterification of renewable oils and blended with petroleum diesel is a promising transportation fuel, and U.S. production reached over 1.2 billion gallons in 2014.[1] A major coproduct of biodiesel production is glycerol, which comprises approximately 10 wt % of the product stream.[2] It is attractive to find processes to upgrade renewable glycerol to more valuable chemicals, therefore improving the feasibility of biodiesel production and reducing our reliance on petroleum feedstock. One promising glycerol conversion route is catalytic hydrogenolysis, which can achieve high selectivity[3−5] to 1,2-propanediol (PDO), a key chemical building block currently produced by petrochemical-based processing of propylene oxide.[6] A recent sustainability analysis found renewable PDO production from glycerol to be a viable and sustainable alternative to the petrochemical route, and this technology has already been commercialized by ADM and BASF.[7] PDO

contains vicinal primary and secondary alcohol groups and may be transformed by oxidation pathways into a wide range of industrially important chemicals, including lactic and pyruvic acids. Oxidation of the primary alcohol group gives lactic acid, which has potential as a major feedstock for sustainable production of polymers, fibers, and solvents,[8,9] while oxidation of the primary and secondary groups yields pyruvic acid, which has seen a rising commercial demand as a health supplement,[10] and also as an important feedstock for chemical, pharmaceutical, and agrochemical industries.[11] Selective oxidation of primary and secondary alcohol groups of PDO through efficient catalytic processes represents an important route for biorenewable chemical production.

Selective oxidation of polyhydric alcohols (polyols) has been a long-term challenge in heterogeneous catalysis, and the dominant factors governing the oxidation of different functional

groups remain unclear. PDO has been studied not only for the industrial significance of its oxidation products but also as a model vicinal-diol molecule for selective oxidation. Initial work by Tsijino et al. demonstrated oxidation of both primary and secondary alcohol groups of PDO using a carbon-supported palladium (Pd/C) catalyst under aqueous conditions (pH 8, 90 °C), showing low selectivity to lactic acid, hydroxyacetone, and pyruvic acid.[12] They found that modifying Pd/C with lead, bismuth, or tellurium gave higher yields of pyruvate via sequential oxidation of lactate. Prati and Rossi compared supported Pd, Pt, and Au catalysts for PDO oxidation by molecular oxygen in alkaline media and found that lactic acid formation was highly selective on these catalysts (89−100%) and occurred through a complex pathway of heterogeneous catalytic steps and homogeneous transformations of inter-mediate species.[13] More recent efforts have focused on optimizing lactic acid yield with Au−Pd,[14] Au−Pt, or Pt−Pd bimetallic catalysts[15] and under mild conditions with an Au−Pt catalyst on activated carbon support.[16]

An alternative to traditional heterogeneous catalysis is to selectively oxidize PDO under electrocatalytic conditions, where the interfacial electrode potential directly affects the Gibbs free energy of reaction and Gibbs chemisorption energy of intermediates.[17] Furthermore, electrocatalytic oxidation in fuel cell reactors offers the potential economic advantage of coproducing electricity and chemical products simultane-ously.[18] Polyols have been investigated as potential fuels because of their high energy densities and wide range of useful oxidation products and may be viable feedstocks for cogeneration if a desired product can be generated with high selectively.[19−29] Horányi and Torkos identified a wide range of oxidation products for PDO on a platinized platinum electrode in acidic media and noted that the reaction scheme is greatly complicated by the simultaneous presence of loosely adsorbed and strongly chemisorbed species on the electrode.[30] Alonso and Gonzalez-Velasco studied the electrooxidation of PDO on a bulk Au plate under basic conditions and identified lactic, acetic, and formic acids as stable products using NMR techniques, while pyruvic acid was not detected.[31] Recently, a PDO-fed organometallic fuel cell was demonstrated, which generated modest electrical power output and lactic acid with total selectivity, achieving simultaneous production of bio-renewable energy and chemicals.[32]

A consistent trend among traditional heterogeneous and electrocatalytic studies has been that oxidation of PDO on Au-based catalysts in alkaline media did not yield significant amounts of pyruvic acid. Our group has investigated the selective electrocatalytic oxidation of polyols on porous carbon cloth supported Pt/C or Au/C electrodes, using glycerol as a model molecule.[23−25,33−35] A key result was the formation of mesoxalate, the product of oxidizing two primary and one secondary alcohol group, was achieved with 46% selectivity on Au/C, while mesoxalate formation was not favored on Pt/C anode catalyst (<3% selectivity).[34] Later, we proposed a reaction intermediate trapping effect after demonstrating that the thick, porous structure of Au/C on carbon cloth supported electrodes facilitated deeper oxidation (to mesoxalate) than thin catalyst layers (<3 μm, on a glassy-carbon rotating disk electrode).[35] On the basis of the similar structures of PDO and glycerol, which both have vicinal primary and secondary alcohol groups, we hypothesized that electrocatalytic oxidation of PDO on a porous Au/C electrode could yield pyruvate analogously

to glycerol oxidation to mesoxalate and reveal more insight into the mechanism and pathway of selective polyol oxidation.

The simultaneous cogeneration of electricity and chemical products (lactate or pyruvate) was demonstrated on self-prepared Pt/C and Au/C anode catalysts in a PDO-fed alkaline anion-exchange membrane fuel cell reactor with ex situ HPLC analysis of liquid products. A custom-made anion-exchange membrane electrocatalytic flow reactor with controllable anode potential was used to study the product selectivity over a wide range of electrode potentials. Linear sweep voltammetry was performed to compare the activity of PDO and proposed intermediate products. A reaction pathway of PDO oxidation for selective formation of lactate or pyruvate was proposed on the basis of results from electrocatalytic experiments and density functional theory (DFT) calculations of reaction energetics over Au(111) and Pt(111) surfaces.

2. METHODS

2.1. Catalyst Synthesis and Characterization. Carbon-supported nanoparticle Pt/C and Au/C catalysts (40 wt %) were synthesized by a solution-phase reduction method. For Au/C synthesis, carbon black (148 mg, Cabot, Vulcan XC-72) was pretreated by refluxing in 4.0 M nitric acid before being dispersed in solution of hexanes and ethanol in an ultrasonic bath. In a separate flask, the metal precursor gold(III) chloride (0.5 mmol, Sigma-Aldrich, 99%) was dissolved in a solution of 1-octadecene (16 mL, Sigma-Aldrich, 90%) and oleylamine (4 mL, Aldrich Chemistry, 70%). The solution was rapidly heated under nitrogen, and a strong reducing agent, lithium triethylborohydride (1.7 mL, Acros Organics, 1.0 M in THF), was quickly injected at 80 °C. The temperature was held for 10 min before cooling in an ice−water bath. The solution was added dropwise to the carbon black mixture under vigorous stirring. Ethanol (800 mL) was pumped slowly into the solution for 10 h. Catalyst was recovered by vacuum filtration and rinsed with ethanol to remove surfactants and solvents. Finally, the catalyst was dried overnight in a vacuum oven at 50 °C. For Pt/C synthesis, pretreated carbon black (146 mg) was dispersed directly in benzyl ether (20 mL, Acros Organics) by ultrasonication, followed by the addition of platinum(II) acetylacetonate (0.5 mmol, Acros Organics, 97%) under magnetic stirring. The solution was heated under nitrogen, and oleic acid (200 μL, Sigma-Aldrich, 90%) and oleylamine (200 μL) were injected at 60 °C. After the precursors were completely dissolved, the solution was heated rapidly to 120 °C. When the solution was thermally stable, 1.7 mL of lithium triethylborohydride solution was injected. After 30 min, the temperature was increased to 180 °C for 1 h. Finally, the Pt/C was cooled, separated, cleaned, and dried in the same manner as for Au/C. Transmission electron microscopy (TEM) images of the as-prepared catalysts were collected on a JEOL 2010 instrument with an operating voltage of 200 kV. High-resolution TEM (HRTEM) images were collected on a JEOL 2010F instrument with an operating voltage of 300 kV. X-ray diffraction (XRD) patterns were obtained with a Scintag XDS-2000 θ/θ diffractometer using Cu Kα radiation (λ = 1.5406), with a tube current of 35 mA and a tube voltage of 45 kV.

2.2. Anion-Exchange Membrane Electrocatalytic Flow Reactors. PDO oxidation was performed in an anion-exchange membrane fuel cell (AEMFC) in a commercial fuel cell fixture (area 5.0 cm², Fuel Cell Technologies) controlled by a fuel cell test system (850e, Scribner Associates Inc.). The anode catalyst was Pt/C or Au/C blended with PTFE (10 wt % PTFE) in

isopropyl alcohol and applied to a carbon cloth liquid diffusion layer (Fuel Cell Store) with a metal loading of 1.0 mg cm^{-2}. The cathode was prepared with carbon-supported transition-metal catalyst (4020 Series, Acta) blended with ionomer (AS-4, Tokuyama Corp.) and applied directly to an anion-exchange membrane (AEM A-201, Tokuyama Corp.) with a catalyst loading of 1.5 mg cm^{-2}. Carbon paper (T-060, Toray) was used as the cathode gas diffusion layer. An aqueous solution of 1.0 M PDO with 2.0 M KOH was pumped through the anode at 4.0 mL min^{-1} by peristaltic pump (Gilson Minipuls 3), while humidified, high-purity O$_2$ (>99.99%, 30 psi) was fed into the cathode for the oxygen reduction reaction. The anode fuel, cathode fuel, and cell temperatures were maintained at 50 °C. Polarization curves were obtained by scanning current from 0 mA to the limiting condition. Constant cell voltage tests were performed at 0.1 V, where 55 mL of PDO alkaline solution was circulated through the anode chamber in a closed loop for 2 h and the final product solution was analyzed by HPLC. The anode potential was monitored by a Hg/HgO (1.0 M KOH) reference electrode inserted into the anode chamber. All potentials herein are reported with respect to the reversible hydrogen electrode (RHE), calculated as $E_{RHE} = E_{Hg/HgO} + 0.098 + 0.059 \times pH$.[25]

A custom-made anion-exchange membrane (AEM) electrocatalytic flow reactor was built as described in our previous works with controllable anode potential.[35,36] Pt/C and Au/C served as working electrode (anode) catalysts, and Pt/C was used as the counter electrode to catalyze the hydrogen evolution reaction. Carbon cloth liquid diffusion layers and membrane were the same as those used in the AEMFC. A Hg/HgO (1.0 M KOH) reference electrode was inserted directly into the anode compartment, allowing the anode potential to be regulated by potentiostat (Versastat MC, Princeton Applied Research). An aqueous solution of 1.0 M PDO with 2.0 M KOH (25 mL) was circulated in a closed loop through the anode chamber, while 2.0 M KOH circulated through the counter chamber. Solution and reactor temperatures were maintained at 50 °C.

2.3. Product Analyses. Initial and final solutions from AEM-based flow reactors were analyzed by HPLC (Agilent 1100) equipped with an Alltech OA-1000 column operated at 60 °C with 5.0 mM sulfuric acid mobile phase flowing at 0.3 mL min^{-1}. Refractive index (Agilent G1362A) and variable wavelength (Agilent G1314F) detectors were used. Products were identified and quantified by comparison to known standard samples. Acid products are reported in their deprotonated forms because the reactions were carried out under high-pH conditions. Detailed calculations of PDO conversion, product selectivity, and carbon balance are found in the Supporting Information.

2.4. Linear Sweep Voltammetry. Linear sweep voltammetry (LSV) was performed in a glass electrochemical reactor (AFCELL3, Pine Instruments) in a three-electrode configuration. Catalysts were dispersed in isopropyl alcohol by ultrasonication to form a uniform ink (1.0 mg mL^{-1}). With a microsyringe, 20 μL of ink was deposited onto a mirror-polished glassy-carbon rotating disk electrode (Pine Instruments, 5.0 mm diameter). A Hg/HgO (1.0 M KOH) reference electrode and platinum-wire counter electrode were used. Tests were performed at a constant sweep rate of 1.0 mV s^{-1} in a nitrogen-purged solution of potassium hydroxide (Sigma-Aldrich, ≥85%), with and without addition of PDO (Sigma-Aldrich, ≥99.5%), in 18.2 MΩ cm deionized water. Additional

tests were performed with lactic acid (Sigma-Aldrich, ≥98%), pyruvic acid (Sigma-Aldrich, 98%), formic acid (Fisher Scientific, 88%), acetic acid (Fisher Scientific, ≥99.7%), or hydroxyacetone (Sigma-Aldrich, 90%).

2.5. DFT Calculations of Electrocatalytic PDO Oxidation on Au and Pt (111) Surfaces. DFT calculations were performed with the Vienna ab initio simulation program (VASP), a molecular dynamics and ab initio energy program.[37−40] The exchange and correlation energies were calculated using the Perdew−Wang functional form (PW91) of the generalized gradient approximation (GGA).[41] A Monkhorst−Pack grid (3 × 3 × 1) was used for structure optimization, followed by single-point calculations using a 4 × 4 × 1 grid.[42] Forces on the reactant atoms were minimized to values lower than 0.05 eV Å^{-1}. The Au(111) and Pt(111) surfaces were modeled with a 3 × 3 unit cell with four atom layers in a vacuum slab model. The bottom two layers were frozen at their bulk fcc cell optimized positions and the top two layers relaxed during structural optimization.

Reaction energies were determined by evaluating the relative energy of each surface intermediate along the oxidation reaction path as a function of electrode potential. The energy of an electron and proton pair, generated during oxidation elementary steps, was determined using the computational hydrogen electrode model.[43,44] Rather than direct calculation of elementary reaction energies, a state relative energy was defined that can be used to construct an overall reaction energy diagram. We define a relative energy (RE) of any surface intermediate, C$_3$O$_x$H$_y$*, as the reaction energy to convert an adsorbed alkoxy species (C$_3$O$_2$H$_7$*) and a water molecule to oxidation products:

$$C_3O_2H_7* + H_2O \rightarrow C_3O_xH_y* + n(H^+ + e^-)$$
$$+ (3 - x)H_2O \qquad (1)$$
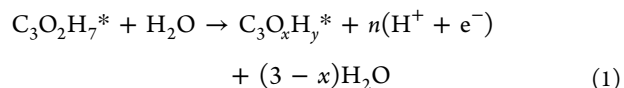
$$RE_{C_3O_xH_y}(U) = E_{C_3O_xH_y*} - E_{C_3O_2H_7*} - E_{H_2O}$$
$$+ (3 - x)E_{H_2O} + \frac{n}{2}G_{H_2} - neU \qquad (2)$$

where E_i represents the DFT energy of a species, G_{H_2} is the free energy of gaseous H$_2$ at standard conditions, e is the absolute value of the elementary electron charge, and U is the electrode potential on the RHE scale. The number of electrons and protons transferred to form the surface intermediate, C$_3$O$_x$H$_y$*, is labeled as n in eqs 1 and 2 and is equal to $3 - y + 2x$. The lowest energy surface alkoxy species (PDO with one alcohol group deprotonated) is used as a reference in generating the reaction energy diagrams. By referencing a surface species, we avoid using an improper reference to a gas-phase propanediol reactant as well as the difficulty of estimating the free energy of the solution-phase propanediol reactant. As solvation of surface species was not considered and the number of strong hydrogen bonds to surface-bound species may differ along the reaction path, conclusions as to dominant reaction paths are only made when differences exceed 0.25 eV.

Nonelectrochemical C−C bond dissociation reactions were also considered on the Au(111) surface. The dissociation reaction energies were calculated with the two dissociated fragments in separate unit cells:

$$\Delta E_{diss} = E_{fragment 1} + E_{fragment 2} - E_{nondissociated} - E_* \qquad (3)$$

where E_* represents the energy of a bare surface site. The dissociation of C−C bonds during PDO oxidation is not formally an oxidation step, and therefore, the C−C dissociation reaction energy is potential independent.

For the surface-bound intermediates, numerous adsorption sites and configurations were considered on the Au(111) surface. Only the most favorable adsorbed configuration and states along the energetically preferred reaction path are reported. Stable optimized structures are illustrated in the Supporting Information, including those on the favored reaction energy path and disfavored structures. The (111) surface was used to model surface chemistry, as it is the lowest energy facet of fcc metals. The experimental catalysts will expose numerous facets, and consideration of the impact of higher index facets on catalytic chemistry is beyond the scope of our current work. As our analysis does not consider activation barriers, and all significant mechanistic conclusions are based on path comparisons that differ by greater than 0.25 eV, the conclusions reached will be relatively robust across surface terminations.

For PDO oxidation on Pt(111), our analysis was limited only to the intermediates found to be along the most preferred path on Au(111), and we presumed adsorption at the most favorable sites located on the Au(111) surface. Our aim was to consider whether differences in energetics along the same path would explain observed kinetic and selectivity differences between the two electrodes, and as discussed later, we conclude that differences in path must occur that are left for future work.

Entropic corrections were not added to the initial PDO or H_2O energies, and therefore the absolute value of the relative energy is less meaningful than the relative values between states. Entropic corrections were not added to surface species, as these are small in comparison to the energy differences of significance in discussing the results. Activation barriers were not calculated and are left as a subject of future work. Though activation barriers would provide greater clarity as to the kinetic differences between catalysts or reaction paths, the reaction energies provided are sufficient to provide useful insight into the experimental results observed.

3. RESULTS AND DISCUSSION

3.1. Catalyst Characterizations. TEM images of self-prepared Pt/C and Au/C catalysts in Figure 1a,c show evenly dispersed, round-shaped nanoparticles on the carbon support, and particle size histograms revealed average particle diameters of 3.1 and 3.0 nm, respectively (Figure S1 in the Supporting Information). HRTEM images shown in Figure 1b,d confirm that the nanoparticles have well-developed crystalline structures. XRD patterns (Figure S2 in the Supporting Information) were collected, and both catalysts displayed typical face-centered cubic (fcc) patterns with diffraction peaks at ca. 39, 46, 65, and 78° assigned to the corresponding (111), (200), (220), and (311) facets, respectively. Average crystal sizes were calculated from the (220) peaks by the Debye−Scherrer formula to be 2.4 and 2.8 nm for Pt/C and Au/C, respectively, which are slightly smaller than average particle diameters calculated from TEM histograms. Cyclic voltammograms were collected in 1.0 M KOH (Figure S3 in the Supporting Information and conform to typical Pt/C and Au/C catalysts prepared by this method.

3.2. PDO Oxidation in AEMFC Reactor. Polarization curves shown in Figure 2a demonstrate that AEMFCs with Pt/C and Au/C anode catalysts can spontaneously oxidize PDO
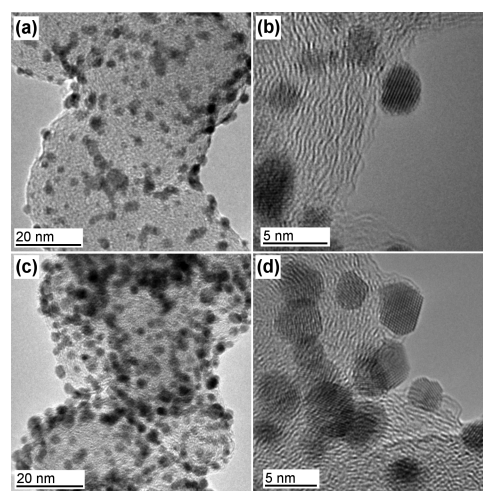
Figure 1. TEM (left) and HRTEM (right) images of Pt/C (a, b) and Au/C (c, d) catalysts.
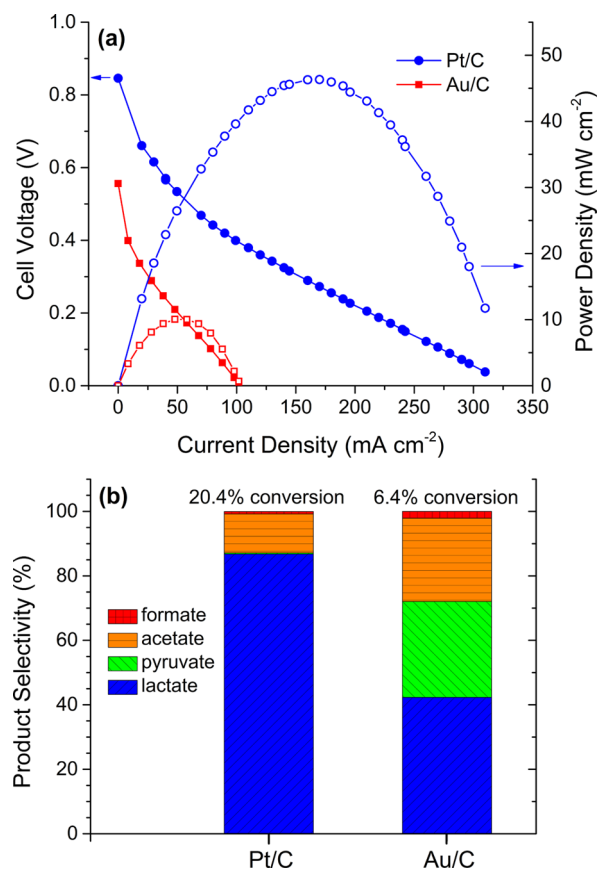
Figure 2. (a) Polarization curves showing cell voltage (solid points) and power density (open points) vs current density in PDO-fed AEMFC and (b) oxidation product distribution after 2 h reaction at a cell voltage of 0.1 V. Conditions: 1.0 M PDO and 2.0 M KOH; 50 °C.

and generate electrical power when they are coupled with the oxygen reduction cathode reaction. The cell had significantly greater open-circuit voltage on Pt/C (0.85 V) in comparison to Au/C (0.56 V), attributed to higher activity and lower activation losses for PDO oxidation on Pt/C. Similarly, peak power density on Pt/C (46.3 mW cm^{-2}) was nearly 5 times greater and limiting current density (310 mA cm^{-2}) was over 3 times greater than those on on Au/C, consistent with reported

results of electrocatalytic oxidation of other polyols in AEMFC, including glycerol and ethylene glycol, on these catalysts.[27,45] Figure 2b reveals the oxidation product profiles as determined by HPLC analysis of the bulk liquid after 2 h of reaction at a controlled cell voltage of 0.1 V. In agreement with the polarization curves, Pt/C showed greater activity for PDO oxidation, reaching about 3 times higher PDO conversion than Au/C. Lactate was the dominant product (86.8%) on Pt/C, while the more deeply oxidized C_3 product pyruvate was detected only in trace amounts (<1%). In contrast, significant amounts of pyruvate (30%) were observed on Au/C. This demonstrates that a PDO-fed AEMFC can coproduce important chemicals (lactate and pyruvate) and electrical power under spontaneous conditions and that product selectivity greatly depends on the anode catalyst. Acetate was the only observed C_2 byproduct, with selectivity ranging from 12 to 26%, which indicates that C−C cleavage occurred under these conditions on both catalysts. It is expected that C−C cleavage would yield equimolar C_1 and C_2 products ($C_3 = C_1 + C_2$); however, formate, the only observed C_1 product, was present in disproportionally low amounts (1−2%). Carbonate is likely another C_1 byproduct, as its presence has been reported in past studies of PDO oxidation,[30] generated either by direct C−C cleavage of C_3 species or by sequential oxidation of formate, although it is not included in this study. Carbon balances ranged from 97 to 99%, as shown in Table S1 in the Supporting Information. Anode potential was monitored during the reactions and averaged 0.39 and 0.49 V vs RHE on Pt/C and Au/C electrodes, respectively. A downfall of the AEMFC setup is that anode potential is limited by the thermodynamics and kinetics of the overall cell and is not directly controlled. To study the effect of changing anode overpotential on the selective electrocatalytic oxidation of PDO, an alternative reactor design was implemented with a three-electrode setup, the AEM-electrocatalytic flow reactor, where the applied anode potential was controlled directly by a potentiostat.

3.3. Electrode Potential Dependent PDO Oxidation.
Selective oxidation of PDO was investigated over a wide range of anode potentials in a custom-made AEM-electrocatalytic flow reactor, utilizing carbon cloth supported Pt/C or Au/C electrodes identical with the AEMFC. A solution of 1.0 M PDO and 2.0 M KOH was cycled through the anode chamber in a closed loop and oxidized at controlled potentials for 1 h. Liquid products were analyzed by HPLC, and the carbon balances ranged from 93 to 99%, as shown in Table S2 in the Supporting Information. All applied potentials (E) reported in this section are with respect to the RHE. Figure 3a shows product profiles of PDO oxidation on Pt/C at applied potentials from 0.2 to 0.7 V. PDO conversion steadily increased with increasing potentials to 12.3% at 0.7 V. Selectivity to lactate was insensitive to anode potential over the tested range, with nearly constant selectivity (86−90%). Acetate and formate were detected in approximately equal amounts at low potentials, but at applied potentials of 0.4 V and higher almost no formate (<1%) was found, which is consistent with results in AEMFC (<1% formate, anode potential 0.39 V). Pyruvate was not detected at potentials lower than 0.4 V and reached a maximum of 1.2% selectivity at the highest potential tested.

Figure 3b shows product profiles of PDO oxidation on Au/C at applied potentials from 0.35 to 0.70 V. The metal loading of Au in the anode catalyst layer was increased from 1.0 to 5.0 mg cm^{-2} to achieve sufficiently high PDO conversion for accurate product analysis. PDO conversion on Au/C was comparable to
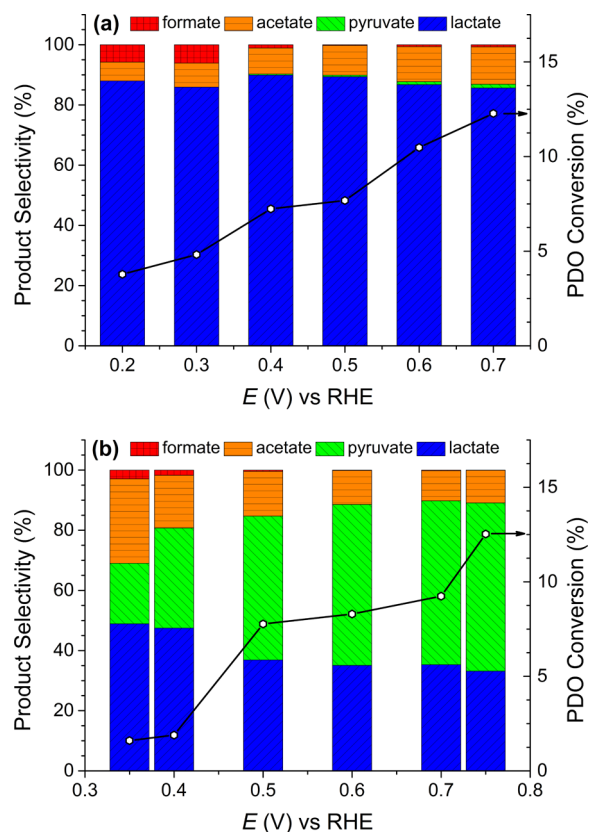

Figure 3. Potential-controlled oxidation of PDO on (a) Pt/C and (b) Au/C in AEM-electrocatalytic flow reactor. Conditions: 1.0 M PDO and 2.0 M KOH; 50 °C; 1 h reaction.

that on Pt/C and increased with increasing applied potentials to a maximum of 12.5% at 0.75 V. Unlike Pt/C, product selectivity on Au/C was strongly dependent on the applied potential. Selectivity to pyruvate, a product not previously obtained from heterogeneous catalytic oxidation of PDO on Au catalysts, increased with increasing potential from 20.1% at 0.35 V to 55.9% at 0.75 V. The increased pyruvate selectivity correlated with decreased lactate selectivity, which dropped from 48.9 to 33.2% with increasing potentials. Acetate was an abundant product (10−28%) at all potentials; however, formate was only detected in substantial quantities at potentials less than 0.6 V. Therefore, it is likely that carbonate, not formate, is the main C_1 product of C−C cleavage at higher potentials. Further investigations of the activity of PDO and proposed reaction intermediates through linear sweep voltammetry and additional AEM-electrocatalytic flow cell reactions were performed to better understand the selective formation of lactate or pyruvate and the distribution of C_1 and C_2 products.

3.4. Linear Sweep Voltammetry of PDO and Proposed Intermediates.
Linear sweep voltammetry (LSV) with a slow sweep rate of 1.0 mV s^{-1} was performed to evaluate the quasi-steady-state current density (j) as a function of potential for alkaline solutions containing PDO and proposed intermediate species. The onset potential was determined as the first potential when oxidation current became greater than the background current in alkaline electrolyte only. PDO oxidation began at significantly more negative potentials on Pt/C than Au/C, which is consistent with open-circuit voltages measured by polarization tests in AEMFC (Figure 2a). Peak current density was reached on Pt/C at 0.69 V, after which the reaction

rate decreases sharply due to formation of surface oxides on the catalyst, which were less active for PDO oxidation. In contrast, peak current density on Au/C occurred at 1.12 V, owing to the higher onset of surface oxide formation on Au.[46] The results indicate that Au/C should be a very active catalyst for PDO oxidation, but large overpotentials are required which were not achieved in the AEMFC reactor.

Figure 4 also shows linear sweep voltammograms in electrolyte containing 0.1 M of the proposed intermediates
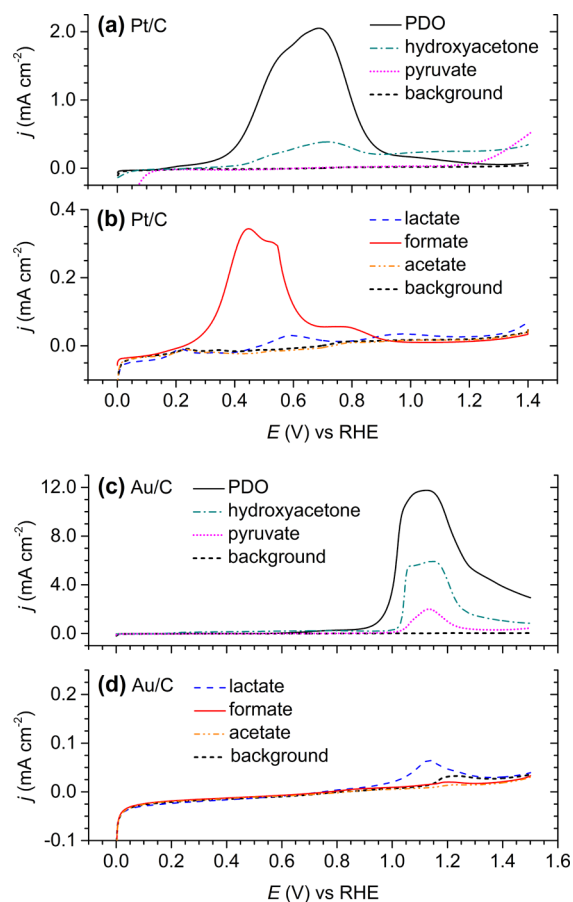
Figure 4. Linear sweep voltammograms recorded at 1.0 mV s^{-1} on (a, b) Pt/C and (c, d) Au/C catalysts of 0.1 M PDO or proposed intermediate products in 1.0 M KOH. The background voltammogram is 1.0 M KOH only.

lactate, pyruvate, hydroxyacetone, formate, and acetate in 1.0 M KOH. Additional alkali was added to neutralize lactic, pyruvic, acetic, and formic acids to keep the effective base concentration constant at 1.0 M. Pyruvaldehyde was not tested, due to its highly unstable nature in alkali.[14] Qualitatively, LSV helps to elucidate the product selectivity observed in AEM-based flow reactors by comparing the reactivities of proposed reaction intermediates and products; however, some variation in onset potentials should be expected due to the different reaction conditions, such as catalyst/substrate ratio, catalyst layer thickness, alkaline/substrate ratio, and temperature.

In Figure 4a, LSV demonstrated that pyruvate was nonreactive on Pt/C until potentials greater than ca. 0.80 V, which is outside the potential range achieved during PDO oxidation in AEM-based reactors, indicating that pyruvate is a stable product on Pt/C which may require PtO$_x$ surface species and large overpotentials to be further oxidized. As previously

shown, lactate was the major product of PDO oxidation on Pt/C in AEM-based reactors; thus, it was surprising that a small oxidation current was observed in the LSV of lactate at moderate potentials (0.4−0.8 V, Figure 4b), indicating that lactate is a slightly reactive product. AEM-electrocatalytic flow cell tests were performed with 1.0 M lactate (Table 1) and

Table 1. Oxidation of Lactate and Pyruvate in AEM-Electrocatalytic Flow Cell[a]

catalyst	anolyte[b]	applied potential (V) vs RHE	conversion (%)	selectivity (%)	product
Pt/C	lactate	<0.5	−	−	−
	lactate	0.5	0.7	100	pyruvate
		0.6	1.0	100	pyruvate
Au/C	lactate	<1.0	−	−	−
		1.0	2.5	98	acetate
		1.1	12.0	100	acetate
		1.2	22.0	100	acetate
Au/C	pyruvate	<1.1	−	−	−
		1.1	28	100	acetate

[a]1 h reaction. [b]Aqueous electrolyte with 1.0 M lactate or pyruvate and 2.0 M KOH.

confirmed that further oxidation of lactate on Pt/C at 0.5 and 0.6 V occurs slowly (lactate conversion ca. 1% after 1 h) and generated pyruvate. Therefore, we hypothesize that the trace amounts of pyruvate (0.3−1.2%) observed from PDO oxidation in Pt/C AEM-based reactors at higher applied potentials resulted from sequential oxidation of readsorbed lactate product. LSV of formate (Figure 4a) showed reactivity at relatively low potentials, which has been previously reported in alkaline media[47] and indicates that further oxidation (to carbonate) is likely. This explains the disproportionally low formate detected on Pt/C in AEM-based reactors. Acetate was found to be nonreactive at all potentials tested on Pt/C; thus, further oxidation of the C$_2$ product is not expected.

LSV on Au/C in Figure 4c,d shows that proposed intermediates have relatively low activity at mild potentials (<1.0 V). The onset potentials of lactate and pyruvate were ca. 0.83 and 0.81 V, respectively, which is outside the potential range tested in AEM-based reactors for PDO oxidation. Oxidation of 1.0 M lactate or pyruvate in alkali was conducted in the AEM-electrocatalytic flow cell, which confirmed that these species are nonreactive on Au/C at potentials less than 1.0−1.1 V, and acetate was the only product detected (Table 1), resulting from C−C cleavage. No activity for acetate and formate oxidation was observed by LSV, and further conversion of these products is not expected in the AEM-based reactors. The relative stability of formate on Au/C supports the hypothesis that carbonate, not formate, is the main C$_1$ product of C−C cleavage at higher potentials and explains the disproportionally low selectivity to formate in AEM-based reactors. LSV of hydroxyacetone (Figure 4c) showed the highest reactivity among proposed C$_3$ intermediates with a very low onset potential of ca. 0.15 V, a sharp current increase at ca. 1.0 V, and two unresolved peaks at 1.06 and 1.14 V. The complexity of the voltammogram could be related to the instability of hydroxyacetone, which is in tautomeric equilibrium with lactaldehyde in alkaline solution through an enediol intermediate.[13] ^{1}H NMR analysis found that the equilibrium of hydroxyacetone and lactaldehyde strongly favors lactaldehyde at pH 12 and higher (Table S3 in the Supporting Information).

Therefore, it is likely that the low onset potential observed in LSV is attributed to aldehyde oxidation of lactaldehyde to lactate. Low onset potentials for aldehyde oxidation (e.g., 0.31 V) have been reported on Au/C in alkaline media.[36] It is likely that hydroxyacetone is a reactive intermediate on Au/C but was not detected in product analysis of PDO oxidation because of its instability under alkaline conditions.

3.5. Proposed Reaction Intermediates and Pathways.

On the basis of evidence from product analysis in electro-catalytic flow reactors and linear sweep voltammetry of PDO and intermediate species, we propose that Pt/C has a preference to oxidization of the primary alcohol group of PDO through the O1 pathway of Scheme 1, producing lactate

Scheme 1. Reaction Network of PDO Oxidation to Lactate and Pyruvate through O1 and O2 Pathways in Alkaline Solution
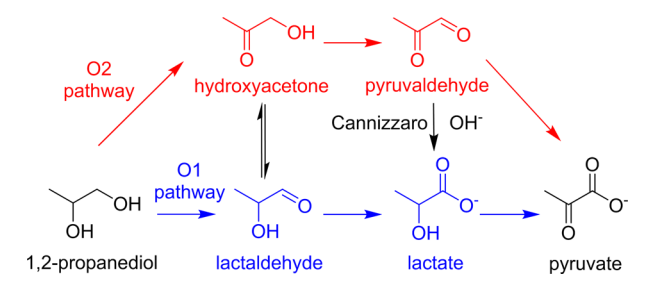

with high selectivity. Formation of lactaldehyde is presumably much slower than its oxidation rate and was not observed in a product analysis of liquid products. Lactate accumulates in the bulk liquid and then very slowly forms pyruvate through secondary alcohol oxidation. C−C bond cleavage occurs with low selectivity to form acetate, a stable product on Pt/C, formate, which can be further oxidized under these conditions, or carbonate, which is not included in this study.

On Au/C, lactate is the main product at low applied potentials but pyruvate becomes more abundant at higher potentials. Since lactate is not further oxidized to pyruvate on Au/C, the pyruvate observed from PDO oxidation is most likely derived from hydroxyacetone by the O2 pathway of Scheme 1. Hydroxyacetone has been a proposed intermediate of PDO oxidation on Au/C in alkaline media on the basis of evidence from H/D exchange experiments[13] and from in situ FTIR spectroscopy.[48] Under oxidizing conditions, Prati and Rossi observed completely selective conversion of hydrox-yacetone to lactate on Au/C and hypothesized that hydroxyacetone is either oxidized to pyruvaldehyde and then transformed to lactate through an intramolecular Cannizzaro reaction or that hydroxyacetone is in equilibrium through an enediol intermediate with lactaldehyde, and the latter is rapidly oxidized to lactate.[13] We propose that the intermediates hydroxyacetone and pyruvaldehyde, which are not stable in high-pH electrolyte, can be further oxidized to pyruvate on Au/C only if they are trapped (long residence times) within the thick liquid diffusion layer of the carbon cloth supported catalyst layer. Electrocatalytic oxidation is accelerated with increasing anode potentials and becomes more competitive with the homogeneous reactions, thus explaining the increased pyruvate selectivity shown in Figure 3b. Additionally, high current densities give rise to decreased local pH within the catalyst layer from the consumption of hydroxide during oxidation reactions,[26] which may delay the base-catalyzed

homogeneous transformations. We hypothesize that the thick electrode structure is crucial for pyruvate formation, which explains why pyruvate has not been reported on Au/C previously on using catalyst dispersed in solution,[13,14,41] a thin layer of Au/C on a glassy-carbon electrode,[48] or an Au plate (polycrystalline Au) electrode.[31] Our related study on the selective oxidation of glycerol on Au electrodes demonstrated that a thick catalyst layer was required to oxidize both primary and secondary alcohol groups to mesoxalate.[35] In fact, no mesoxalate was observed on thin catalyst layers (<3 μm, on glassy-carbon electrode). Direct evidence of the O2 pathway to pyruvate is not confirmed, as neither hydroxyacetone nor pyruvaldehyde were identified by product analysis, likely attributed to their instability in the bulk alkaline solution. Furthermore, equilibrium between lactaldehyde and hydrox-yacetone makes a definite determination of the preferred pathway to pyruvate challenging without the use of rigorous theoretical calculations or advanced techniques such as in situ spectroscopy, which should be a focus of future studies.

3.6. Electrochemical Oxidation Mechanism on Au and Pt by DFT.

The electrocatalytic selective oxidation of PDO was studied using DFT calculations to identify the most favorable reaction intermediates and provide more evidence of the likely path of the potential-dependent PDO oxidation on Au and Pt catalysts. The electrocatalytic oxidation of alcohol functional groups in alkaline media is largely believed to undergo an initial deprotonation step catalyzed by OH⁻ in the electrolyte, followed by metal-catalyzed C−H and C−C bond breaking steps, which require the Au catalyst.[49] Therefore, DFT calculations were performed by starting from either the adsorbed terminal oxygen alkoxy (O1) or the secondary oxygen alkoxy (O2) on Au(111) or Pt(111), both presumed to form following a solution-mediated oxidative deprotonation step. Oxidations of up to six electrons to form pyruvic acid were considered, mainly considering C_3 products. C−C dissociation is considered on the Au(111) surface. All potentials referred to in this section are with respect to the RHE.

Figure 5a depicts the reaction energy diagram for PDO oxidation over the Au(111) surface at 0 V. All preferred structures, as well as nonpreferred structures and intermediates considered, are depicted in Table S4 in the Supporting Information. Blue lines connect states reasonably connected by elementary reaction steps beginning with deprotonation and adsorption of primary alkoxide (O1), whereas red lines are for reactions initiated at the secondary position (O2). All reactions considered as elementary steps involve transfer of a single electron and breaking (deprotonation) or formation (C−OH formation) of a single bond on the surface intermediate. As the reaction energy diagrams in Figure 5 reference the adsorbed alkoxy species, the generally weak binding of intermediates to the Au(111) surface is not evident. Without free energy corrections to the solvated propanediol reactant state, we cannot directly determine an equilibrium coverage of any species on the surface. We instead resort to a reference to the gas-phase species to illustrate the lack of favorability of adsorption to the Au(111) surface and encourage the reader to recognize that additional free energy corrections would act to further destabilize a surface-bound state in comparison to a fluid-phase state. The O2 alkoxy species ($+H^+ + e^-$) is 1.39 eV higher in energy than gas-phase PDO at 0 V, and all species are at positive energies relative to the gas-phase PDO species at 0 V. This suggests that the Au surface will be devoid of PDO reaction intermediates at 0 V, in agreement with the lack of an
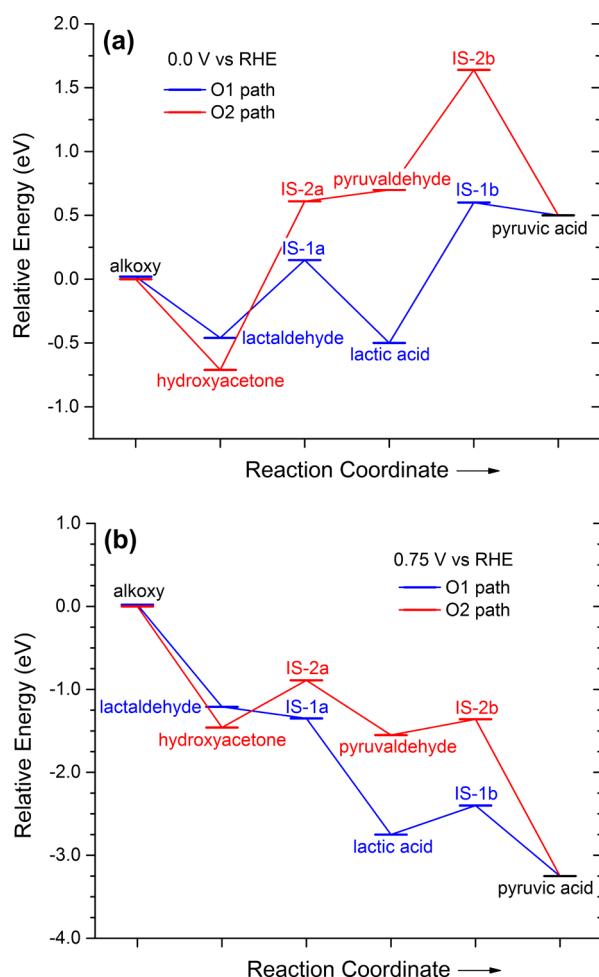
Figure 5. Reaction free energy diagrams of PDO oxidation through the O1 and O2 pathways at (a) 0.0 V and (b) 0.75 V on the Au(111) surface.

oxidation current at this potential. At 0.75 V, the initial alkoxy species remains 0.64 eV higher in energy than a gas-phase PDO reference, suggesting that a low coverage of this initial reactive intermediate may limit the oxidation rate. Formation of oxidation surface intermediates beyond the initial alkoxy species is favorable at 0.75 V, confirming that favorable oxidation may occur at this potential, in agreement with an experimentally observed oxidation current.

Formation of lactaldehyde, lactic acid, and pyruvic acid follow from progressively deeper oxidation of the initial O1-bound alkoxy species. On binding through O1, the terminal oxygen, lactaldehyde is formed by favorable C−H breaking of the alkoxide. Though this elementary reaction energy is favorable, this step can be expected to have a significant activation barrier at 0 V. Further oxidation breaks another primary C−H bond, generating an intermediate state (IS-1a, $CH_3−CHOH−C*O$, where the asterisk indicates a direct interaction with the surface). The formation of this intermediate state is unfavorable, uphill in energy by 0.61 eV at 0 V, suggesting that lactate formation requires an overpotential to be accessible on the Au(111) surface. Formation of a C−OH bond (and oxidizing H_2O) to lactic acid is then favorable from the unstable IS-1a state. Further oxidation to pyruvic acid requires breaking a secondary C−H bond to form IS-1b ($CH_3−C*OH−COOH$). Formation of IS-

1b from lactic acid has a reaction energy of 1.10 eV at 0 V, and the overall formation of pyruvic acid from lactic acid is unfavorable, corroborating the experimental results that lactate is the major product at low potentials.

If PDO is initially deprotonated at the secondary position, forming an alkoxide bound through O2, initial C−H breaking to form hydroxyacetone is highly favorable. Further oxidation from hydroxyacetone, which is found to preferentially occur through breaking a primary C−H bond, requires a large energy input of 1.324 eV at 0 V to reach IS-2a ($CH_3−CO−C*HOH$). Though formation of hydroxyacetone (O2 path) is slightly thermodynamically favorable over lactaldehyde (O1 path), further oxidation of hydroxyacetone requires multiple high-energy steps to proceed. At low potentials, any hydroxyacetone formed would likely prefer the homogeneous transformation to lactaldehyde via tautomerism and then further oxidization through the O1 path. Further oxidations to pyruvaldehyde and through IS-2b to pyruvic acid are also unfavorable at low potentials. Pyruvaldehyde would be rapidly transformed to lactic acid through a homogeneous Cannizzaro reaction under alkaline conditions, as previously reported,[13] rather than continue on the O2 reaction path.
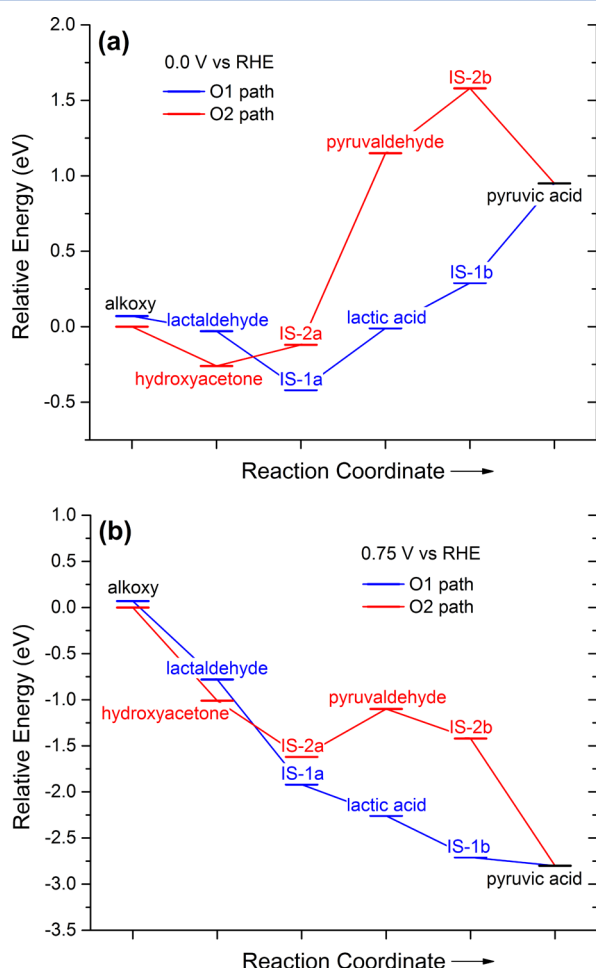
Figure 5b illustrates the PDO oxidation reaction energy diagram over the Au(111) surface at 0.75 V. At the higher potential, oxidation through the O1 path to lactic acid is favorable for all elementary steps. Oxidation of lactic acid to pyruvic acid appears favorable at this potential, though an uphill step through IS-1b remains. Both the O1 and O2 paths to pyruvic acid become more accessible as the potential increases, in agreement with the experimentally observed increase in pyruvate selectivity. Formation of IS-1b on the O1 path requires an uphill energy of 0.35 eV at 0.75 V. Both IS-2a (0.57 eV) and IS-2b (0.20 eV) require surmounting uphill energy steps to reach pyruvic acid along the O2 path at 0.75 V. Therefore, on the basis of the DFT calculations and experimental evidence, we propose that lactic acid formation on Au/C can form via two paths, binding through either the primary or secondary alcohols. At low potentials, lactic acid is the only viable stable oxidation product on Au electrodes. At higher overpotentials, DFT results suggest both the O1 and O2 paths to pyruvic acid on Au become viable, with the energetic differences too close (within 0.25 eV) to discern a preference, given the lack of solvation and single Au surface termination considered. Combining these considerations with the experimental observation that lactic acid does not oxidize at low potentials on Au electrodes (Table 1), we conclude that the O2 path to pyruvic acid becomes operable at higher oxidation potentials.

Table 2 gives the C−C dissociation reaction energies for all intermediates along the reaction path in Figure 5. Structures of adsorbed C−C bond dissociation fragments are included in Table S5 in the Supporting Information. Most C−C dissociation energies are endothermic, indicating a general lack of activity of the Au(111) surface for C−C dissociation. For the one species that showed exothermic C−C dissociation energies (IS-2b), its oxidation reaction in Figure 5a is more favorable and therefore likely to compete against C−C dissociation. The increasing selectivity to C_3 products with increasing anode potential in the flow reactor (Figure 3) is consistent with the increased rate of oxidation relative to C−C dissociation, as well as the DFT results indicating that later oxidation intermediates do not show enhanced tendency toward C−C dissociation.

Table 2. C−C Bond Dissociation Reaction Energies (eV) of PDO Oxidation Intermediates on the Au(111) Surface

species	fragment 1	fragment 2	ΔE_{diss}
alkoxy-1	CH_3-CHOH	CH_2O	0.83
lactaldehyde	CH_3-CHOH	CHO	1.79
IS-1a	CH_3-CHOH	CO	1.12
lactic acid	CH_3-CHOH	COOH	1.96
IS-1b	CH_3-COH	COOH	2.40
pyruvic acid	CH_3-CO	COOH	1.05
alkoxy-2	CH_3-CHO	CH_2OH	0.04
hydroxyacetone	CH_3-CO	CH_2OH	1.29
IS-2a	CH_3-CO	CHOH	1.02
pyruvaldehyde	CH_3-CO	CHO	0.72
IS-2b	CH_3-CO	CHOOH	−0.80

Figure 6 illustrates the reaction energy diagrams for PDO oxidation over the Pt(111) surface, and structures of all surface

Figure 6. Reaction free energy diagrams of PDO oxidation through the O1 and O2 pathways at (a) 0.0 V and (b) 0.75 V on the Pt(111) surface.

intermediates are illustrated in Table S6 in the Supporting Information. Relative to a gas-phase PDO species, the O2-bound alkoxy species (+0.93 eV) and all subsequent intermediates are unstable at 0 V, in agreement with the lack of an observed oxidation current at low overpotentials. All intermediates bind more strongly to Pt(111) than to Au(111), and all surface intermediates past the initial alkoxy species (0.18

eV) are stable relative to gas-phase PDO at 0.75 V. Differences in intermediate binding are especially evident for the unstable (IS-1a, IS-1b, IS-2a, and IS-2b) intermediate states, with all elementary steps on the O1 path being downhill in energy at 0.75 V on Pt(111). The stronger binding of the unstable intermediates demonstrates the greater activity of the Pt catalyst, as the potential limiting steps of forming the IS states on Au are all more favorable on Pt. This agrees with the greater observed oxidation currents for Pt in comparison to those for Au electrodes.

Mechanistic causes of selectivity differences between Au and Pt catalysts, specifically Au forming pyruvate at higher potentials whereas Pt is selective to lactate, are not evident from the reaction energy diagrams. Pt(111) shows a more favorable formation of IS-1b for transformation of lactate to pyruvate at lower overpotentials in comparison to the Au(111) surface. The mechanistic source of this selectivity difference must stem from factors not considered in this study, which could include higher index facets of the surface, activation barriers not correlated with reaction energies, surface coverage or electrolyte effects, or differences in reaction paths between Au and Pt not considered herein. We speculate that the surface coverage of intermediates during PDO oxidation will differ significantly between Au and Pt electrodes and that this is a likely cause of the selectivity differences. Numerous C_1 to C_3 intermediates could form, bind strongly on the Pt surface, and be resistant to rapid oxidation. A higher coverage of surface intermediates on the Pt surface could drive preferential oxidation at the terminal carbon atom, as the terminal carbon atom could more easily access a surface site in a high-coverage environment than the sterically inhibited secondary carbon. Direct consideration of coverage effects is beyond the scope of this study but provides an interesting direction for future consideration of selective oxidation of PDO.

4. CONCLUSIONS

PDO-fed alkaline anion-exchange membrane fuel cells successfully cogenerated electricity and valuable chemical products with peak power densities of 46.3 mW cm^{-2} on Pt/C and 10.0 mW cm^{-2} on Au/C. Pt/C was highly selective for primary alcohol group oxidation to lactate (86.8%) under fuel cell conditions with very little activity of secondary alcohol oxidation to pyruvate. Au/C was less active than Pt/C but gave significant amounts of pyruvate (30%), a product that has previously eluded heterogeneous catalytic studies on Au. Pyruvate selectivity on Au/C was sensitive to anode potential and was further increased to 56% by increasing the applied potential in an AEM-electrocatalytic flow reactor. Sequential oxidation of lactate to pyruvate was not observed on Au/C but did occur slowly on Pt/C. On the basis of observed product distributions and linear sweep voltammetry of intermediate products, we proposed that the intermediates hydroxyacetone and pyruvaldehyde, which are not stable in alkaline electrolyte, can be further oxidized to pyruvate on Au/C only if they are trapped within the thick liquid diffusion layer of the carbon cloth supported catalyst layer. We hypothesized that long residence times and local pH effects within the thick electrode structure are crucial for pyruvate formation, which explains why pyruvate has not been previously reported on Au. DFT calculations of reaction energies identified the most favorable reaction intermediates and concluded that the O2 pathway through hydroxyacetone becomes viable at high potentials, which is consistent with the experimentally observed increase in

pyruvate selectivity with applied potential on Au/C. A definitive determination of reaction pathways is challenging due to the instability and interconversion of proposed reaction intermediates and should be a focus of future studies.

■ ASSOCIATED CONTENT

Ⓢ Supporting Information

The Supporting Information is available free of charge on the ACS Publications website at DOI: 10.1021/acscatal.5b01085.

> Detailed calculations of conversion, selectivity, and carbon balance, TEM particle size histograms, XRD patterns, cyclic voltammograms, summary of PDO oxidation in AEMFC and AEM-electrocatalytic cell reactors, ^{1}H NMR analysis of hydroxyacetone/lactaldehyde equilibrium, and optimized intermediate structures and relative energies from DFT (PDF)

■ AUTHOR INFORMATION

Corresponding Authors

*M.J.J.: tel, +1-814-863-9366; fax, +1-814-865-7846; e-mail, mjanik@engr.psu.edu.
*W.L.: tel, +1 515-294-4582; fax, +1 515-294-2389; e-mail, wzli@iastate.edu.

Present Address

$^{||}$(J.Q. and W.L.) Department of Chemical and Biological Engineering, Iowa State University, Ames, IA 50011, United States.

Author Contributions

$^{\perp}$These authors (D.J.C. and L.X.) contributed equally to this work.

Notes

The authors declare no competing financial interest.

■ ACKNOWLEDGMENTS

■ REFERENCES

(1) U.S. Energy Information Administration, Monthly Biodiesel Production Report, July 31, 2015.
(2) Yang, F.; Hanna, M. A.; Sun, R. *Biotechnol. Biofuels* **2012**, *5*, 13−22.
(3) Dasari, M. A.; Kiatsimkul, P.-P.; Sutterlin, W. R.; Suppes, G. J. *Appl. Catal., A* **2005**, *281*, 225−231.
(4) Miyazawa, T.; Kusunoki, Y.; Kunimori, K.; Tomishige, K. *J. Catal.* **2006**, *240*, 213−221.
(5) Maris, E.; Davis, R. *J. Catal.* **2007**, *249*, 328−337.
(6) Martin, A. E.; Murphy, F. H. Glycols, Propylene Glycols. In *Kirk-Othmer Encyclopedia of Chemical Technology*; Wiley: Hoboken, NJ, 2000.
(7) Marinas, A.; Bruijnincx, P.; Ftouni, J.; Urbano, F. J.; Pinel, C. *Catal. Today* **2015**, *239*, 31−37.
(8) Auras, R.; Harte, B.; Selke, S. *Macromol. Biosci.* **2004**, *4*, 835−864.
(9) Datta, R.; Henry, M. *J. Chem. Technol. Biotechnol.* **2006**, *81*, 1119−1129.
(10) Xu, P.; Qiu, J.; Gao, C.; Ma, C. *J. Biosci. Bioeng.* **2008**, *105*, 169−175.
(11) Li, Y.; Chen, J.; Lun, S.-Y. *Appl. Microbiol. Biotechnol.* **2001**, *57*, 451−459.
(12) Tsujino, T.; Ohigashi, S.; Sugiyama, S.; Kawashiro, K.; Hayashi, H. *J. Mol. Catal.* **1992**, *71*, 25−35.
(13) Prati, L.; Rossi, M. *J. Catal.* **1998**, *176*, 552−560.
(14) Dimitratos, N.; Lopez-Sanchez, J. A.; Meenakshisundaram, S.; Anthonykutty, J. M.; Brett, G. L.; Carley, A. F.; Taylor, S. H.; Knight, D. W.; Hutchings, G. J. *Green Chem.* **2009**, *11*, 1209−1216.
(15) Ryabenkova, Y.; Miedziak, P. J.; Dummer, N. F.; Taylor, S. H.; Dimitratos, N.; Willock, D. J.; Bethell, D.; Knight, D. W.; Hutchings, G. J. *Top. Catal.* **2012**, *55*, 1283−1288.
(16) Ryabenkova, Y.; He, Q.; Miedziak, P. J.; Dummer, N. F.; Taylor, S. H.; Carley, A. F.; Morgan, D. J.; Dimitratos, N.; Willock, D. J.; Bethell, D.; Knight, D. W.; Chadwick, D.; Kiely, C. J.; Hutchings, G. J. *Catal. Today* **2013**, *203*, 139−145.
(17) Vuyyuru, K. R.; Strasser, P. *Catal. Today* **2012**, *195*, 144−154.
(18) Alcaide, F.; Cabot, P.-L.; Brillas, E. *J. Power Sources* **2006**, *153*, 47−60.
(19) Yuan, X.; Ma, Z.; Bueb, H.; Drillet, J. F.; Hagen, J.; Schmidt, V. M. *Electrochim. Acta* **2005**, *50*, 5172−5180.
(20) Bambagioni, V.; Bianchini, C.; Marchionni, A.; Filippi, J.; Vizza, F.; Teddy, J.; Serp, P.; Zhiani, M. *J. Power Sources* **2009**, *190*, 241−251.
(21) Simões, M.; Baranton, S.; Coutanceau, C. *Appl. Catal., B* **2010**, *93*, 354−362.
(22) Simões, M.; Baranton, S.; Coutanceau, C. *ChemSusChem* **2012**, *5*, 2106−2124.
(23) Zhang, Z.; Xin, L.; Li, W. *Appl. Catal., B* **2012**, *119−120*, 40−48.
(24) Zhang, Z.; Xin, L.; Li, W. *Int. J. Hydrogen Energy* **2012**, *37*, 9393−9401.
(25) Qi, J.; Xin, L.; Chadderdon, D. J.; Qiu, Y.; Jiang, Y.; Benipal, N.; Liang, C.; Li, W. *Appl. Catal., B* **2014**, *154−155*, 360−368.
(26) Han, X.; Chadderdon, D. J.; Qi, J.; Xin, L.; Li, W.; Zhou, W. *Int. J. Hydrogen Energy* **2014**, *39*, 19767−19779.
(27) Xin, L.; Zhang, Z.; Qi, J.; Chadderdon, D.; Li, W. *Appl. Catal., B* **2012**, *125*, 85−94.
(28) Qi, J.; Xin, L.; Zhang, Z.; Sun, K.; He, H.; Wang, F.; Chadderdon, D. J.; Qiu, Y.; Liang, C.; Li, W. *Green Chem.* **2013**, *15*, 1133−1137.
(29) Marchionni, A.; Bevilacqua, M.; Bianchini, C.; Chen, Y. X.; Filippi, J.; Fornasiero, P.; Lavacchi, A.; Miller, H.; Wang, L.; Vizza, F. *ChemSusChem* **2013**, *6*, 518−528.
(30) Horanyi, G.; Torkos, K. *J. Electroanal. Chem. Interfacial Electrochem.* **1981**, *125*, 105−113.
(31) Alonso, C.; Gonzalez-Velasco, J. *J. Electroanal. Chem. Interfacial Electrochem.* **1988**, *248*, 193−208.
(32) Bellini, M.; Bevilacqua, M.; Filippi, J.; Lavacchi, A.; Marchionni, A.; Miller, H. A.; Oberhauser, W.; Vizza, F.; Annen, S. P.; Grutzmacher, H. *ChemSusChem* **2014**, *7*, 2432−2435.
(33) Zhang, Z.; Xin, L.; Qi, J.; Wang, Z.; Li, W. *Green Chem.* **2012**, *14*, 2150−2152.
(34) Xin, L.; Zhang, Z.; Wang, Z.; Li, W. *ChemCatChem* **2012**, *4*, 1105−1114.
(35) Zhang, Z.; Xin, L.; Qi, J.; Chadderdon, D. J.; Sun, K.; Warsko, K. M.; Li, W. *Appl. Catal., B* **2014**, *147*, 871−878.
(36) Chadderdon, D. J.; Xin, L.; Qi, J.; Qiu, Y.; Krishna, P.; More, K. L.; Li, W. *Green Chem.* **2014**, *16*, 3778−3786.
(37) Kresse, G.; Hafner, J. *Phys. Rev. B: Condens. Matter Mater. Phys.* **1993**, *47*, 558−561.
(38) Kresse, G.; Hafner, J. *Phys. Rev. B: Condens. Matter Mater. Phys.* **1994**, *49*, 14251−14269.
(39) Kresse, G.; Furthmüller, J. *Comput. Mater. Sci.* **1996**, *6*, 15−50.
(40) Kresse, G.; Furthmüller, J. *Phys. Rev. B: Condens. Matter Mater. Phys.* **1996**, *54*, 11169−11186.
(41) Perdew, J. P.; Chevary, J. A.; Vosko, S. H.; Jackson, K. A.; Pederson, M. R.; Singh, D. J.; Fiolhais, C. *Phys. Rev. B: Condens. Matter Mater. Phys.* **1992**, *46*, 6671−6687.
(42) Monkhorst, H. J.; Pack, J. D. *Phys. Rev. B* **1976**, *13*, 5188−5192.

(43) Yeh, K. Y.; Janik, M. J. Density Functional Theory Methods for Electrocatalysis. *Computational Catalysis*; The Royal Society of Chemistry: London, 2014; Chapter 3.

(44) Nørskov, J. K.; Rossmeisl, J.; Logadottir, A.; Lindqvist, L.; Kitchin, J. R.; Bligaard, T.; Jónsson, H. *J. Phys. Chem. B* **2004**, *108*, 17886−17892.

(45) Zhang, Z.; Xin, L.; Qi, J.; Chadderdon, D. J.; Li, W. *Appl. Catal., B* **2013**, *136−137*, 29−39.

(46) Kwon, Y.; Schouten, K. J. P.; Koper, M. T. M. *ChemCatChem* **2011**, *3*, 1176−1185.

(47) John, J.; Wang, H.; Rus, E. D.; Abruña, H. D. *J. Phys. Chem. C* **2012**, *116*, 5810−5820.

(48) Bott-Neto, J. L.; Garcia, A. C.; Oliveira, V. L.; de Souza, N. E.; Tremiliosi-Filho, G. *J. Electroanal. Chem.* **2014**, *735*, 57−62.

(49) Kwon, Y.; Lai, S. C.; Rodriguez, P.; Koper, M. T. *J. Am. Chem. Soc.* **2011**, *133*, 6914−6917.